buildings

MDPI

Article

Effects of Carbon Thin Film on Low-Heat Cement Hydration, Temperature and Strength of the Wudongde Dam Concrete

Haoyang Peng [1], Peng Lin [1,*], Yunfei Xiang [1], Jinwu Hu [2] and Zongli Yang [2]

[1] Department of Hydraulic Engineering, Tsinghua University, Beijing 100084, China; phyang1994@163.com (H.P.); xiangyf20@mails.tsinghua.edu.cn (Y.X.)
[2] China Three Gorges Corporation, Beijing 100038, China; hu_jinwu@ctg.com.cn (J.H.); yang_zongli@ctg.com.cn (Z.Y.)
* Correspondence: celinpe@tsinghua.edu.cn

Abstract: Research on the mechanism of carbon thin film (CTF) is a hot issue in the field of concrete materials and is of great significance to the temperature control and crack prevention of concrete structures, but little research has been conducted regarding this issue. In this paper, the composition of CTF and its influence on cement hydration, concrete temperature and strength are studied in the context of the Wudongde (WDD) dam project. Through observations of hand specimens, rock slice identification and X-Ray Fluorescence (XRF) analysis, it was shown that the CTF has the same chemical composition as the limestone component, except for the presence of low-crystalline graphite. Based on hydration testing using TAM Air, it was found that CTF promotes the dissolution of cement and the hydration of C3A in the very early stage but exerts a lowering effect on the second exothermic peak of cement hydration. In addition, the greater the CTF content, the greater the hydration heat release. According to temperature measurements of the Wudongde (WDD) dam, CTF could promote an increase in the maximum temperature of concrete blocks. Finally, compressive strength analysis revealed that the content of CTF was proportional to the compressive strength of concrete specimens and provides a reference for the effect of CTF on the performance of low-heat cement concrete.

Keywords: carbon thin film; low-heat cement; hydration; concrete strength; super high arch dam

check for updates

Citation: Peng, H.; Lin, P.; Xiang, Y.; Hu, J.; Yang, Z. Effects of Carbon Thin Film on Low-Heat Cement Hydration, Temperature and Strength of the Wudongde Dam Concrete. *Buildings* **2022**, *12*, 717. https://doi.org/10.3390/buildings12060717

Academic Editor: Shazim Memon

Received: 28 April 2022
Accepted: 24 May 2022
Published: 26 May 2022

1. Introduction

The phenomenon of concrete dam cracking is widely prevalent and is caused by load-transfer and stress redistribution within the dam shell and abutments [1–3], and by progressive thermal stresses exceeding the tensile strength of mass concrete or tensile strains exceeding the ultimate tensile strain. Control of cracking in a dam is essential for the long-term safety and stability of the dam, particularly in the case of super high arch dams [2–4]. The raw material factors affecting the formation of concrete cracks can be classified into effects due to aggregate properties or due to cement hydration.

Generally, the aggregate accounts for about 80% of the volume of concrete in a dam and therefore has a significant influence on the concrete strength and risk of cracking. Concrete aggregates are of various types, grading, sizes, shapes, coefficients of thermal expansion (CTE), strengths and propensities for alkali reactions to occur. Studies indicated that the type of aggregate affects the performance of concrete [5]. Grey granite aggregate, for example, has produced concrete with the highest compressive strength, fracture energy and modulus of elasticity, followed by Anorthosite, Charnockite, Limestone and Gneiss [6]. Aggregate grading also affects ASR damage and the quality of concrete. A 10% grading deviation from the ASTM C1293 Standard for a reactive coarse aggregate could lead to up to a 50% increase in concrete expansion [7]. It has been shown that, as aggregate size increases, the tensile strength of the resultant concrete decreases but the fracture energy increases. Additionally, the elasticity modulus of concretes made with strong matrix–aggregate interfaces decreases as the aggregate size increases [8]. In addition,

the tensile strength, fracture energy and elastic modulus of concretes made with angular aggregates have been shown to be slightly higher than those for concretes made with spherical aggregates [9]. It has also been found that concrete's CTE, which increases with aggregate's CTE, greatly affects the development of thermal cracks in concrete. A finer aggregate grading can slightly increase the concrete's CTE [10]. In addition, the increase in concrete strength with the strain rate is higher for limestone aggregate concrete containing a relatively low-strength coarse aggregate than for siliceous aggregate concrete containing very strong siliceous aggregates [11]. Moreover, alkali–aggregate reactions bring about harmful concrete expansion and loss of stiffness, which can lead to excessive deterioration, undesirable deformations and cracking of the concrete [12–15].

In addition to the aggregate properties, the enormous amount of heat generated by cement hydration has a significant impact on dam cracking. To reduce the heat generated by the cement hydration process, admixtures are usually incorporated within cement, such as limestone powder, slag, fly ash, silica powder, graphene oxide, etc. Earlier research has indicated that, when cement is blended with admixtures, its hydration process can be significantly affected. It has been shown that limestone powder promotes the initial cement hydration reaction stage [16] and affects the hydrate composition of cement pastes [17]. The presence of fine-grained limestone leads to hydrocarboaluminate calcium formation [18] and the incorporation of limestone causes a transformation of monosulfoaluminate into monocarboaluminate in the hydration product at 28 days at 5 and 23 °C [19]. In addition, the hydration heat release rate and total heat release have been found to be influenced by the particle size of the limestone powder [20]. A finer limestone powder can increase the size of the exothermic peak and advance the time of its occurrence [21]. Slag characteristics also play a very important role in the process of cement hydration [22]. It has been shown that limestone and slag powder rapidly reduce the hydration heat of cement, especially the initial stage hydration heat, and shorten the induction period [23]. The cumulative heat release of cement paste hydration decreases as the nickel slag content increases due to the low pozzolanic activity of nickel slag [24]. Furthermore, phosphorus slag was found to delay the hydration process of cement and inhibit the formation of ettringite [25]. It has also been shown that fly ash could reduce the hydration rate of OPC and total heat release [26–28]. The hydration of cement clinker is affected by fly ash, which accelerates the long-term hydration of Alite, although it delays the hydration reaction of Belite and C_4AF [29]. In the presence of both calcium hydroxide and fly ash, the hydration reaction increases because calcium hydroxide provides an additional nucleation site [27]. It has also been found that blending cement with metakaolin in binary blends increases the heat release rate while fly ash does not [21]. The hydration reaction of cement containing fly ash accelerates when limestone powder is incorporated [30]. There are also studies that indicate that fine silica powder particles accelerate the hydration process [31,32]. Furthermore, graphene oxide promotes the hydration reaction because of its nucleation effect [33,34]. Therefore, it can be stated that aggregate properties and different admixtures directly affect the performance of concrete and dam cracking risks.

In the Wudongde (WDD) Hydropower Station, carbon thin film (CTF) has been found in the limestone aggregate [35]. The CTF is a thin film mixture containing carbon and its composition analysis is detailed in Section 2.2. Although the presence of CTF within limestone aggregates of dam concrete is common, little research has been conducted on its effects on concrete properties. The related studies found so far are as follows: at Shuibuya Hydropower Station, the low gas content of the concrete has been mainly attributed to the raw sand containing a certain amount of CTF, which has an adsorption effect on the air entraining agent and reduces the bleed air effect [36]; at Liyang Pumped Storage Power Station, the amount of water and cement required was found to increase when the concrete included limestone sand containing CTF [37]; in addition, the carbonaceous limestone aggregate at Fengweihe Hydropower Station produced concrete of poor robustness and durability [38]. These studies are the first to consider the effects of CTF on concrete.

However, the impacts of different CTF contents on low-heat cement hydration and concrete compression strength have not yet been systematically studied and evaluated.

In this study, firstly, the source of the aggregate containing the CTF, its composition and the challenges posed to the concrete performance of the WDD dam are introduced. Then, the specific effects of the CTF on the hydration rate and heat of the low-heat cement are investigated based on hydration testing using TAM Air. In addition, the influence of the CTF on the actual concrete temperature is analyzed by comparing the measured concrete temperature of the WDD dam and the results of the hydration test. Finally, compressive strength tests of four-grade concrete with different CTF contents are carried out and the influence of CTF on the concrete strength of the WDD dam is analyzed. This study provides a reference for the effect of CTF on the performance of low-heat cement concrete.

2. Site Geological Investigation on Aggregate Field

2.1. The WDD Aggregate Field

The WDD Hydropower Station is located in Luquan county in southwest China and is under construction. The Hydropower Station includes a double-curvature arch dam (height 270 m), a spillway tunnel and an underground power generation system. The installed electrical capacity is 10.2 million kilowatts. The WDD Hydropower Station is located in a dry and hot river valley, with large temperature differences in the mornings and evenings, and a maximum temperature difference of 14 °C. Therefore, temperature control when pouring concrete is challenging, requiring strict control of the aggregate properties to avoid dam cracking over time.

In the Shiqi aggregate field (Figure 1a), karst has not developed, and the limestone rock mass shows good integrity and abundant reserves (about 6.515 million m^3, which is 2.5 times the amount required for the dam). Furthermore, the Shiqi aggregate field is only about 6 km from the dam site, and its upstream area is adjacent to the storage field (the linear distance is approximately 0.8 km). Therefore, the limestone in the Shiqi aggregate field offers a great source of dam concrete aggregate for the WDD Hydropower Station. The Shiqi aggregate production system is shown in Figure 1b.

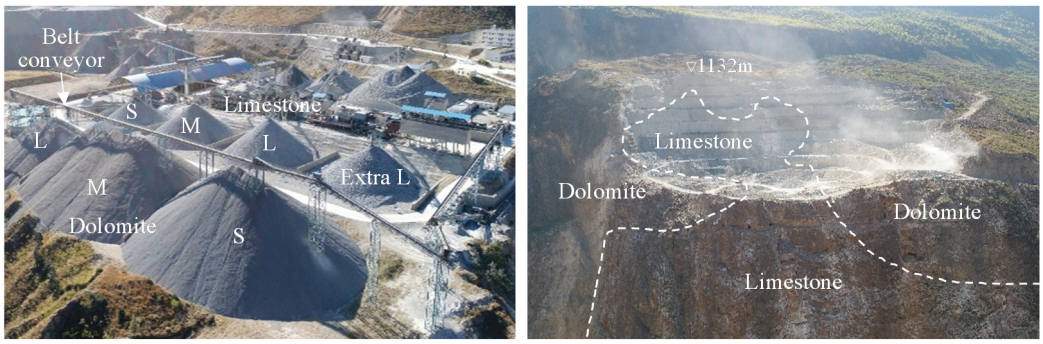

(**a**) (**b**)

Figure 1. Shiqi aggregate system at WDD hydropower station: (**a**) Shiqi aggregate field; (**b**) Shiqi aggregate production system (Note: L is the large stone, M is the medium stone, S is the small stone, Extra L is the extra-large stone).

In 2017, after the aggregate production system of the WDD Hydropower Station had produced limestone aggregates, a layer of black grease-stained film material was seen floating on the surface of the wastewater draining from the sand. The main mineral components and chemical composition of this black grease, and the question of whether it will affect the performance of the dam concrete, have received extensive attention. Figure 2a shows the distribution of CTF at EL 1027 m~1040 m at the Shiqi aggregate field. The present form of the CTF is shown in Figure 2b,c.

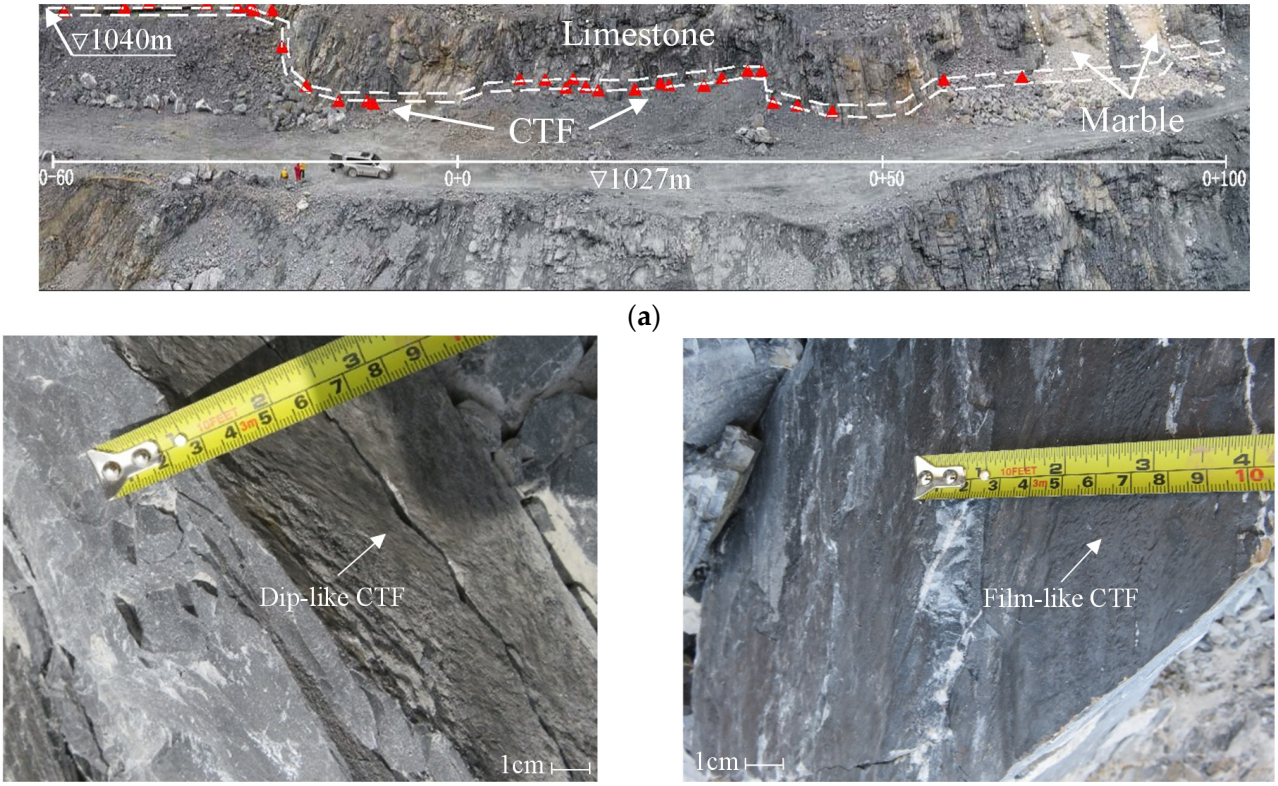

Figure 2. Distribution and present form of CTF in the limestone: (**a**) Distribution of the CTF; (**b**) Dip-like CTF; (**c**) Film-like CTF.

2.2. Composition of the CTF

The CTF used in this study was derived from the Shiqi aggregate production system at the WDD Hydropower Station. Based on observation of hand specimens made of the CTF (Figure 3a) and identification of rock slices (Figure 3b), the main properties of the CTF are as follows: (1) The CTF is between 0.005 and 0.1 mm thick, has a certain metallic luster and stains hands, resulting in a slippery feel. (2) The film layer on the rock surface contains a certain amount of carbonaceous material, of content not more than 10%. (3) The carbonaceous material consists of irregularly shaped particles smaller than 5 μm, distributed in the interior of the calcite particles and between the particles. The red arrows in Figure 3b represent pyrite particles.

An analysis of 25 samples was conducted using X-Ray Fluorescence (XRF) imaging to provide the maximum, minimum and average content of each composite in the CTF, and these findings are shown in Table 1. Based on observation of the hand specimens, rock slice identifications and XRF analyses, the CTF was shown to have the same chemical composition as the limestone component, with the addition of low-crystalline graphite.

Table 1. Determining the composition of the CTF by XRF analysis method (% by weight).

Component	MgO	Al_2O_3	SiO_2	P_2O_5	S	K_2O	CaO	Ti	Mn	Fe
Content (%)	3.90	13.60	28.13	0.28	1.94	5.69	10.15	1.77	0.02	1.86

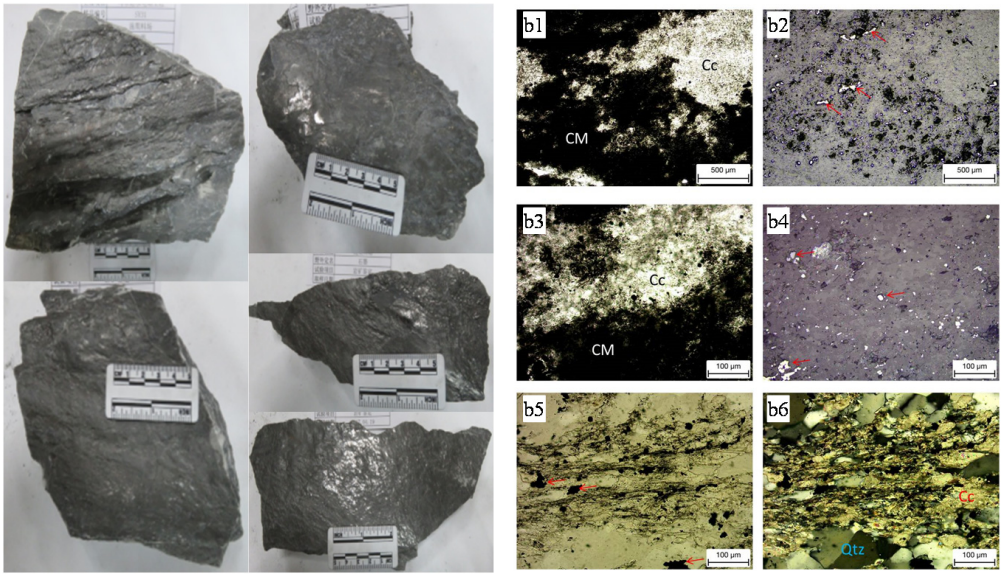

(**a**) (**b**)

Figure 3. Composition analysis of the CTF: (**a**) Visual observation of CTF hand specimens; (**b**) Rock slice identification.

2.3. Main Problem of Aggregate

The WDD Hydropower Station is a millennium project and has the seventh highest capacity worldwide. Concrete quality is the most important guarantee of dam quality, concrete performance and long-term stability. The limestone containing the CTF from the Shiqi aggregate field was the best choice of aggregate with all other factors considered. A thorough study the effect of CTF on the physical properties and construction properties of the WDD dam concrete was essential and presented a big challenge. In particular, it was necessary to study the effects of CTF on physical and chemical stability during the cement hydration process, the impact on the cement hydration process and the effect on the concrete strength and cracking interface. These studies were conducted understand the potential influence of the CTF on concrete quality and reduce the risk of cracking of the WDD dam concrete.

3. Experimental Program

During this study, a series of hydration experimental studies investigating the effects of the CTF on the hydration rate, hydration heat produced and hydration evolution process were carried out. In addition, 28d compressive strength tests of four-grade concrete with different CTF contents were carried out simultaneously. The specimen material preparation, experimental system, analysis cases and test processes are introduced in this section.

3.1. Materials and Mixture Proportions

The materials used in the hydration test were as follows. The low-heat cement raw material was P.LH42.5 cement from the Sichuan Jiahua Huidong Company (China), and the main mineral components by weight were C_3S (30.15%), C_2S (43.568%), C_3A (0.978%) and C_4AF (15.702%). The main chemical components of the low-heat cement are given in Table 2. The CTF derives from the limestone aggregate at the Shiqi field. After the limestone aggregate had been crushed, washed and sieved, the CTF was mainly concentrated in the production system waste water (Figure 4), and was collected from that waste water by filtering.

Table 2. Chemical components of low-heat cement (% by weight).

Component	SiO_2	Al_2O_3	Fe_2O_3	CaO	MgO	SO_3	Loss	K_2O
Content (%)	23.06	3.674	5.164	59.76	4.55	2.012	0.778	—

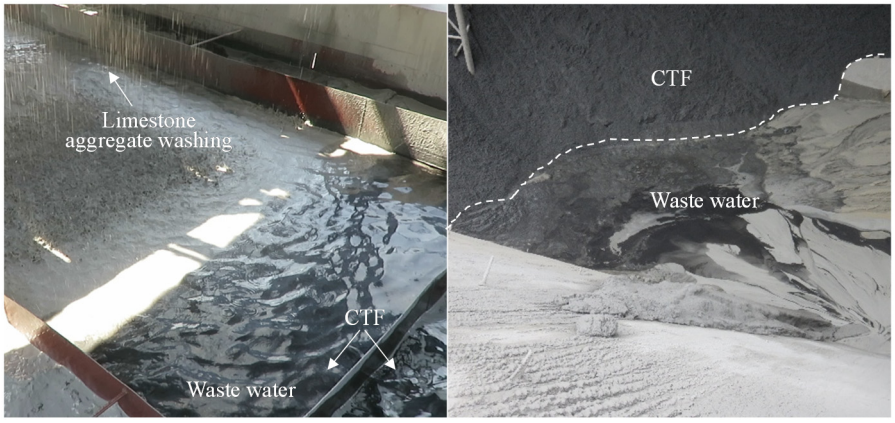

Figure 4. Collection of the CTF at WDD Hydropower station.

The compressive strength test adopted a $C_{180}30$ four-grade concrete mixture. The cement was the same as that used in the hydration test. The coarse and fine aggregate was from the Shiqi aggregate field. The fly ash was Qujing Fangyuan grade I and the mixing amount was 35%. The water–binder ratio was 0.5, and the sand rate was 24.8%. The theoretical mixing amount of 1 m^3 concrete is shown in Table 3.

Table 3. The theoretical mixing amount of four-grade concrete.

Material	Low-heat Cement	Fly Ash	Sand	Stone				Admixtures		Water
				Small	Medium	Large	Extra Large	JM-II 0.6%	GYQ 0.025%	
Mixing amount Kg/m^3	108	58	574	348	348	522	522	0.996	0.042	83

3.2. Experimental System

An isothermal heat conduction calorimetry (TAM Air) test system, ASTM C1702-13 was employed to investigate the low-heat cement hydration heat evolution process with different quantities of the CTF. The TAM Air is an air-based thermostat that uses heat sinks to conduct heat from the specimens and minimize external temperature disturbance. The thermostat uses a circulating air and advanced temperature control system to maintain a high degree of temperature stability (ranging within ±0.02 K). The specimen is placed in an ampoule in contact with the heat flow sensor, and the heat flow sensor is in contact with the heat sink. As long as heat is generated or heat is dissipated during the reaction, a temperature gradient is generated at the sensor, producing a voltage, which is recorded. This voltage is proportional to the heat flow in the sensor and the rate of reaction of the specimen in the ampoule. The calorimeter records the voltage signal continuously and in real time.

Compressive strengths were determined in accordance with the DL/T5150-2017 Test code for hydraulic concrete using 450 mm cubes stored in saturated limewater until the testing stage. A 15 MN universal testing machine was used to load the cubes. The curing temperature of the concrete specimens was controlled at 20 ± 5 °C, and the relative humidity was not less than 90%.

3.3. Analysis Cases and Test Processes

The hydration reaction of cement is exothermic. Although the period of cement hydration heat release is very long, most of that heat is released within 3 days. Therefore, all analyses were performed during the first 3 days of hydration at a control temperature of 25 °C. The hydration heat and its rate of generation were recorded every 22 s by the TAM Air apparatus. The reference value of the content of CTF in the paste test was 4/100,000 of the cement content and the water-cement ratio was 0.5. A total of 12 specimens divided into 6 groups were prepared. The specimens, with different CTF content, are shown in Table 4.

Table 4. Test specimens in cement paste with different content of the CTF.

Name	Number	Water (g)	Cement (g)	CTF (mg)	Remarks
WDD-JJ12	2	2.89	5.78	0	Plain cement
WDD-JJB3-4	2	2.89	5.78	0.2312	1X CTF
WDD-JJB5-6	2	2.89	5.78	0.6936	3X CTF
WDD-JJB7-8	2	2.89	5.78	11.0976	48X CTF
WDD-JJB9-10	2	2.89	5.78	13.872	60X CTF
WDD-JJB11-12	2	2.89	5.78	23.12	100X CTF

Note: X indicates that the content of CTF accounts for 4/100,000 of the amount of low-heat cement.

The hydration test flow includes seven steps (Figure 5), which were as follows: weighing the CTF; weighing the deionized water; mixing the low-heat cement with CTF; mixing the low-heat cement, CTF and water in the ampoule; applying a "muddler' to the mixture; sealing the ampoule with a capping machine; and, finally, measuring the hydration heat generated and its rate of generation in the TAM Air apparatus.

The strength tests with 0, 1 and 60 times CTF contents were designed to study the influence of CTF on the strength performance of concrete. Among them, 0X content of CTF is the reference group, 1X content of CTF is the average content in sand aggregate, namely the possible content of CTF in the WDD dam concrete, and 60X content is set because 60X content was found to have great influence on cement hydration heat based on the results of the hydration test.

Three specimens were used as a group to test the compressive strength of the four-grade concrete. The test scheme is shown in Table 5. The 15 MN universal testing machine was used to continuously and uniformly load (without impact) at a speed of 6 MPa/min until the specimen was destroyed, and the failure load was recorded (Figure 6).

Table 5. Compressive strength test of four-grade concrete with different CTF contents.

Name	Size mm^3	Number	CTF		Age d
			Times	Mass (g)	
WDD-C1~3	450^3	3	0X	0	28
WDD-C4~6		3	1X	2.00854	
WDD-C7~9		3	60X	120.51245	

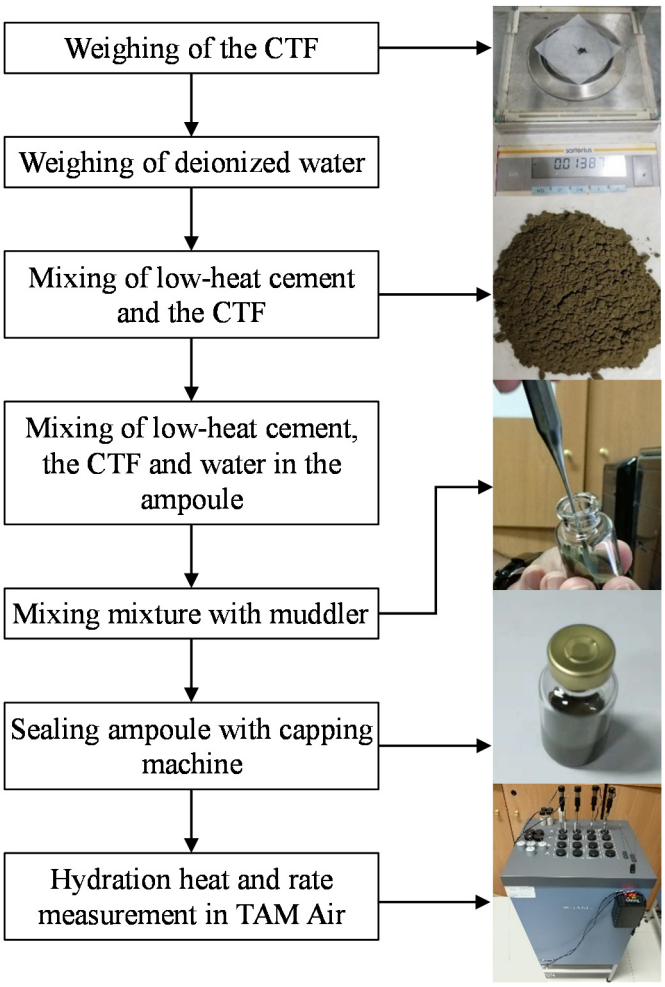

Figure 5. The hydration test flow.

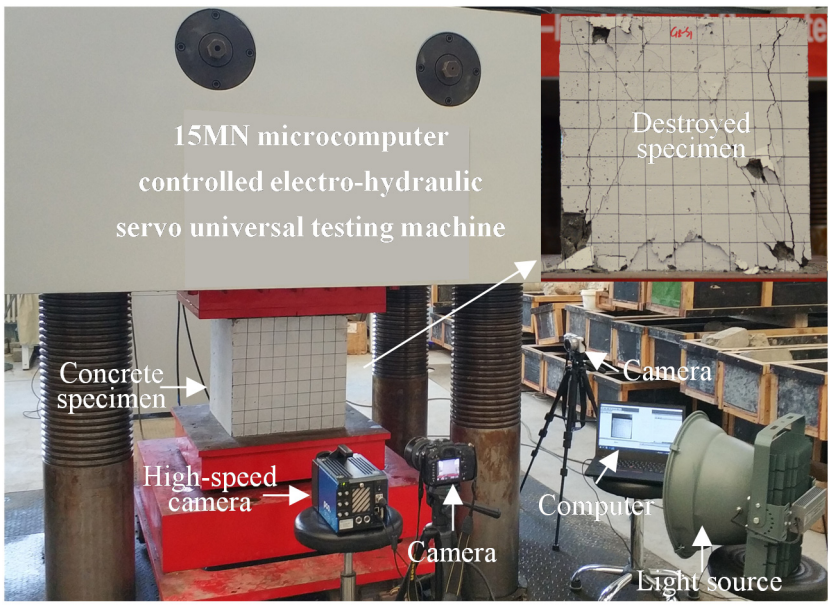

Figure 6. Compressive strength test processes of the four-grade concrete.

4. Results and Discussion

4.1. Effects of the CTF on Hydration Rate and Heat

(1) Effects of the CTF on hydration rate

Figure 7 shows the evolution of the heat release rate process from 0 to 72 h, as obtained experimentally from the hydration tests. For different amounts of CTF mixed with a constant amount of low-heat cement and water, the evolution of the overall heat release rate was basically the same, with all curves having the four obvious stages of initialization, induction, acceleration and deceleration. The arrival times and durations of each stage are basically consistent. Based on the experimental analysis results, the following could be observed: (1) at 24 h, the differences between the heat release rates of a pure cement specimen and specimens 1X, 3X, 48X, 60X and 100X were −0.6, −1.2, −0.6, −0.9 and 0.6%, respectively ("−" indicates a lower rate than for the pure cement specimen); (2) at 48 h, the differences in the exothermic rates were −1.5, −1.0, 0.7, −3.3 and 1.1%, respectively; (3) at 72 h, the differences in the exothermic rates were −1.8, −0.7, 1.1, −4.2 and 3.3%, respectively. In summary, the hydration heat release rates were similar for all specimens. With the increase in the content of CTF, the rate of heat release does increase (except for the 60X samples), but the increase is not large. In the final, 72 h, stage, 1X, 3X and 60X showed a relatively reduced rate of hydration heat release, while 48X and 100X showed a relatively increased rate.

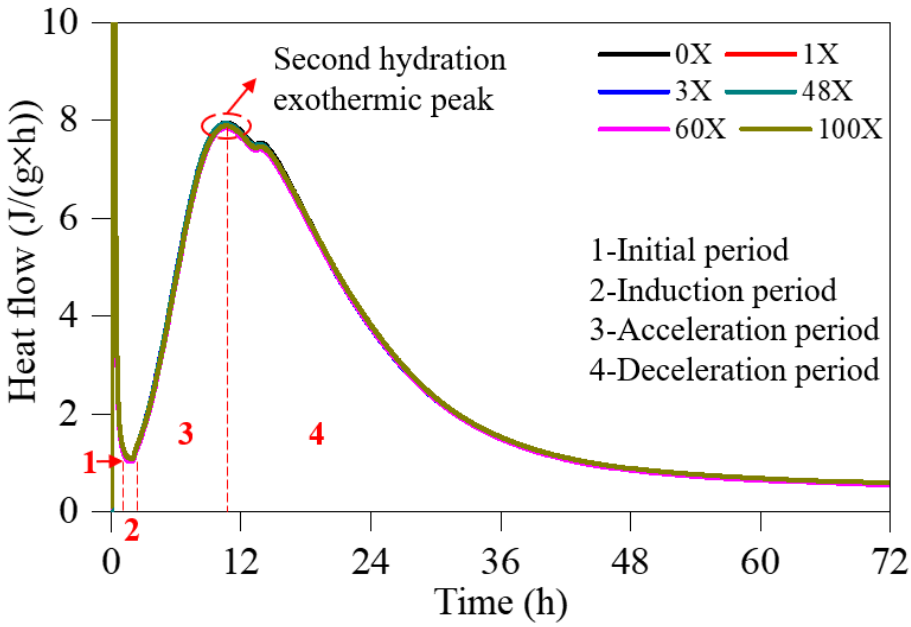

Figure 7. Evolution of heat release rate from 0 to 72 h with different contents of the CTF.

Figure 8a shows the first hydration exothermic peak for each specimen. The first exothermic peak is due to the quick dissolution of aluminate and sulfate [39]. After about 3 min, all specimens, all with different CTF contents, reached the first exothermic peak, but the rate of exothermic heat generation varied greatly for each specimen. At the first peak, the differences in the rate of heat generation between the pure cement specimen and specimens 1X, 3X, 48X, 60X and 100X were 12.0, 30.0, 21.3, 56.7, and 52.0%, respectively. This indicates that the CTF can promote the dissolution of cement and the hydration of C_3A in the early stage, and the higher the content of CTF, the faster the rate of hydration heat release. However, increasing the amount of CTF does not proportionally increase the hydration heat release rate.

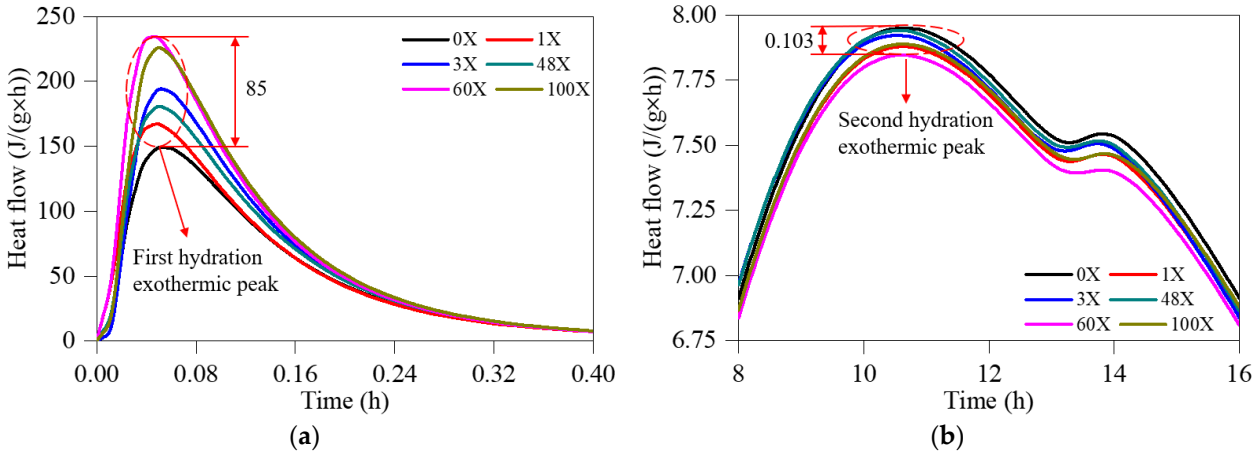

Figure 8. Hydration exothermic peak with different content of the CTF: (**a**) First hydration exothermic peak; (**b**) Second hydration exothermic peak.

The second hydration exothermic peak for each specimen is shown in Figure 8b. After about 10.5 h, the specimens, with different CTF content, reached the second exothermic peak. The second exothermic peak is mainly caused by the rapid hydration of C_3S, to form $Ca(OH)_2$ and C-S-H gel [27,39]. There is a smaller shoulder after the second exothermic peak due to the interconversion between AF_t and AF_m [40]. The differences between the pure cement specimen and specimens 1X, 3X, 48X, 60X and 100X at the time of the second exothermic peak were −0.9, −0.3, −0.1, −1.3, and −0.8%, respectively, and the second exothermic peaks of all specimens containing the CTF were smaller than the peak for the pure cement specimen. These findings indicate that the CTF slows down the rate of hydration generation leading to the second peak, but the reduction is small.

(2) Effects of the CTF on hydration heat

Figure 9 shows the hydration heat process curves from 0 to 72 h. It can be seen from Figure 9 that, after mixing different amounts of CTF with equal amounts of low-heat cement and water, the overall heat release rates were similar. However, there was an overall trend: as the CTF content increased, the heat released increased. At 24 h, the differences between the cumulative heat released for the pure cement specimen and specimens 1X, 3X, 48X, 60X and 100X were 0.4, 2.5, 2.0, 4.1 and 4.6%, respectively. At 48 h, the differences were 0.1, 1.0, 1.5, 2.8 and 3.7%, respectively. At 72 h, they were −0.1, 1.4, 1.5, 2.3 and 3.6%. This shows that the CTF increases the cumulative heat release of low-heat cement hydration and indicates that the greater the CTF content, the more the hydration heat increases.

In the initial stage of heat release (within the first hour), the hydration heat release increases with the increase in the CTF content. The cumulative heat releases of the 60X, 100X specimens are the greatest. The pure cement specimen releases the least amount of heat.

During 48–72 h, the hydration heat release of specimens 0X and 1X were close to each other and the heat release for 3X and 48X were also similar to one another. The specimen 100X produced the greatest hydration heat release. The difference between the maximum heat release and the minimum was stable at 7.5 (J/g), indicating that the CTF promotes an increase in the release of cement hydration heat in the early stage and later, but that heat release is not linearly proportional to the CTF content.

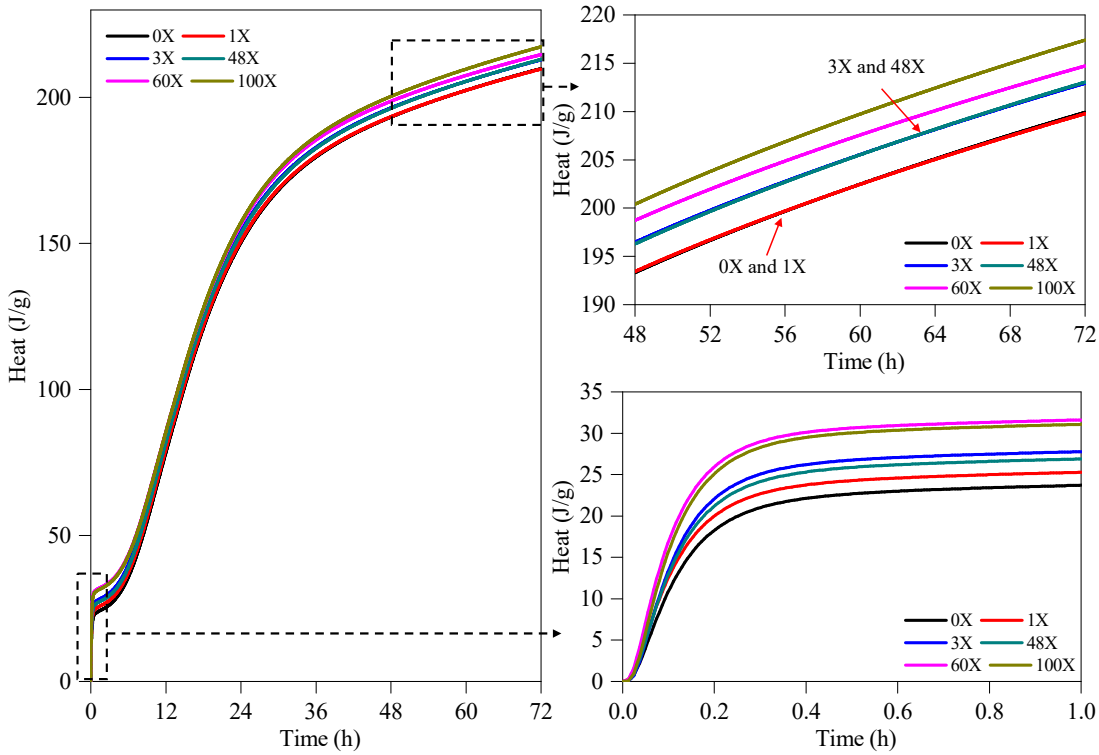

Figure 9. Hydration heat release process from 0 to 72 h with different content of the CTF.

(3) Evolution process of the CTF in low-heat cement hydration

The application of TAM Air isothermal calorimeter techniques revealed that the hydration of the low-heat cement was accelerated in the presence of the CTF. The evolution process of CTF in the low-heat cement hydration is demonstrated in Figure 10. This process involves a hydrophobic effect, a nucleation effect and a chemical reaction effect.

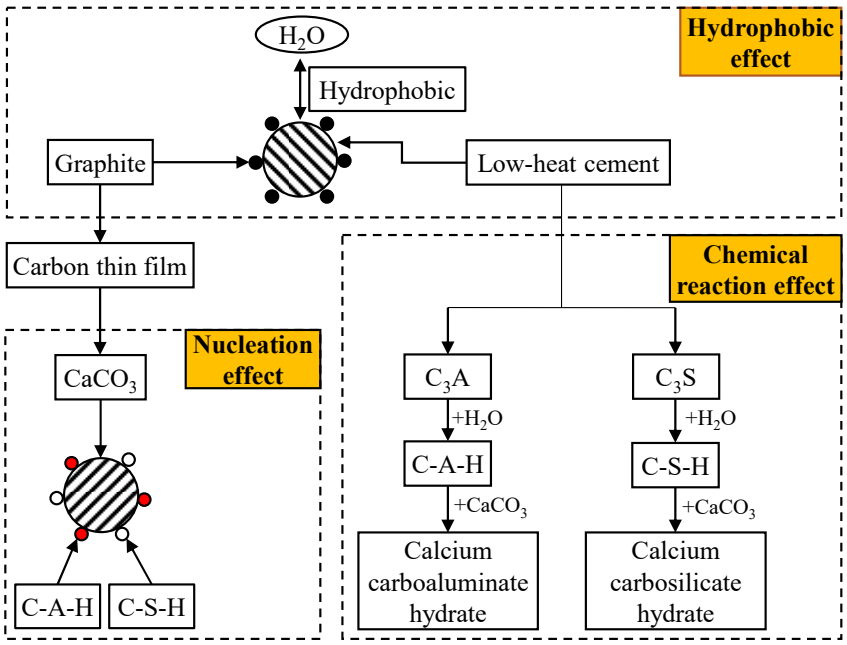

Figure 10. The evolution process of the CTF in low-heat cement hydration.

The hydrophobic effect means that, in the low-heat cement hydration process, the graphite present in the CTF retards the cement hydration reaction. The graphite disperses

in the cement matrix in a non-uniform manner, due to an aggregation, or collecting together, effect. Because of the hydrophobic nature of graphite, those cement particles aggregating to the graphite have less access to water for hydration reaction purposes [41], thereby reducing the rate of the reaction overall, and resulting in a corresponding increase in the hydration time of the low-heat cement.

The nucleation effect occurs because the limestone powder can act as a nucleation site during the cement hydration reaction, inducing crystallization of the hydration products and promoting cement hydration [17,23,42]. On the one hand, $CaCO_3$ particles act as nucleation sites to induce crystallization of C_3A hydration products and accelerate cement hydration. The nucleation of calcium carbonate particles promotes the growth of a large amount of C_3A hydration products on the surface, resulting in a decreased ion concentration in the solution. Thereby, the ions on the surface of the C_3A particles migrate into the solution quickly and the hydration rate of C_3A increases. On the other hand, when C_3S begins to hydrate, a large amount of Ca^{2+} is released into the solution. Ca^{2+} has a much higher migration ability than the $SiO_4{}^{4-}$ ions. According to the adsorption theory, when Ca^{2+} diffuses to the vicinity of $CaCO_3$ particle surfaces, the adsorption of Ca^{2+} on the surface of the $CaCO_3$ particles occurs first. Due to this adsorption, the concentration of Ca^{2+} around the C_3S particles is lowered, enabling the hydration process of C_3S to accelerate.

The chemical reaction effect entails that, on the one hand, C_3A from the low-heat cement reacts rapidly with water to form calcium aluminate hydrate. The calcium aluminate hydrate then reacts with $CaCO_3$ within the CTF to form calcium carboaluminate hydrate ($C_3A{\cdot}CaCO_3{\cdot}11H_2O$), which promotes the cement hydration process [23,43]. On the other hand, C_3S forms C-S-H when it mixes with water, and calcium carbonate reacts with C-S-H to form calcium carbosilicate hydrate, which accelerates the hydration of C_3S [44].

4.2. Effect of the CTF on the Dam Concrete Temperature

In July 2017, at the commencement of CTF aggregate mining in the WDD hydropower station, the concrete contained more CTF, at a content of about 1X~3X, because improvements to the aggregate's production and cleaning process had not yet been completed. In April 2019, the intensity of the aggregate flushing process was increased to reduce the CTF content in the concrete (close to 0X) to prevent the CTF from adversely affecting the concrete performance. For this reason, the concrete temperatures during July, August, November and December in 2017 and 2019 were selected when exploring the influence of the CTF on the concrete temperature of the WDD dam. Based on the temperature change curves (Figure 11) and statistics on the highest temperature of the concrete blocks (Table 6), the results show the following: (1) The concrete blocks with a lower CTF content reached their highest temperature at a lower age, with the ages in July, August, November and December being shorter by 0.2 d, 0.3 d, 14.3 d and 17.1 d, respectively. This indicates that the hydration rate of concrete blocks with a lower CTF content was faster. (2) Comparing the years 2017 and 2019, the highest temperatures of the concrete blocks in July and August reached maximum, minimum and average values of 27.3 °C, 25.7 °C and 26.55 °C, versus 27.3 °C, 21.3 °C and 24.84 °C, respectively. The average highest temperature of the concrete blocks in July and August 2017 was about 1.71 °C higher than that in July and August 2019. (3) Comparing the years 2017 and 2019, the highest temperatures of the concrete blocks in November and December reached maximum, minimum and average values of 26.6 °C, 25 °C and 26.09 °C versus 26.76 °C, 20.24 °C and 23.36 °C, respectively. The average highest temperature of the concrete blocks in November and December 2017 was about 2.73 °C higher than that in November and December 2019. The highest temperature of the concrete blocks containing more CTF content (2017) was generally higher than that of the concrete blocks containing less CTF content (2019), which demonstrates that CTF could promote the release of heat from cement hydration.

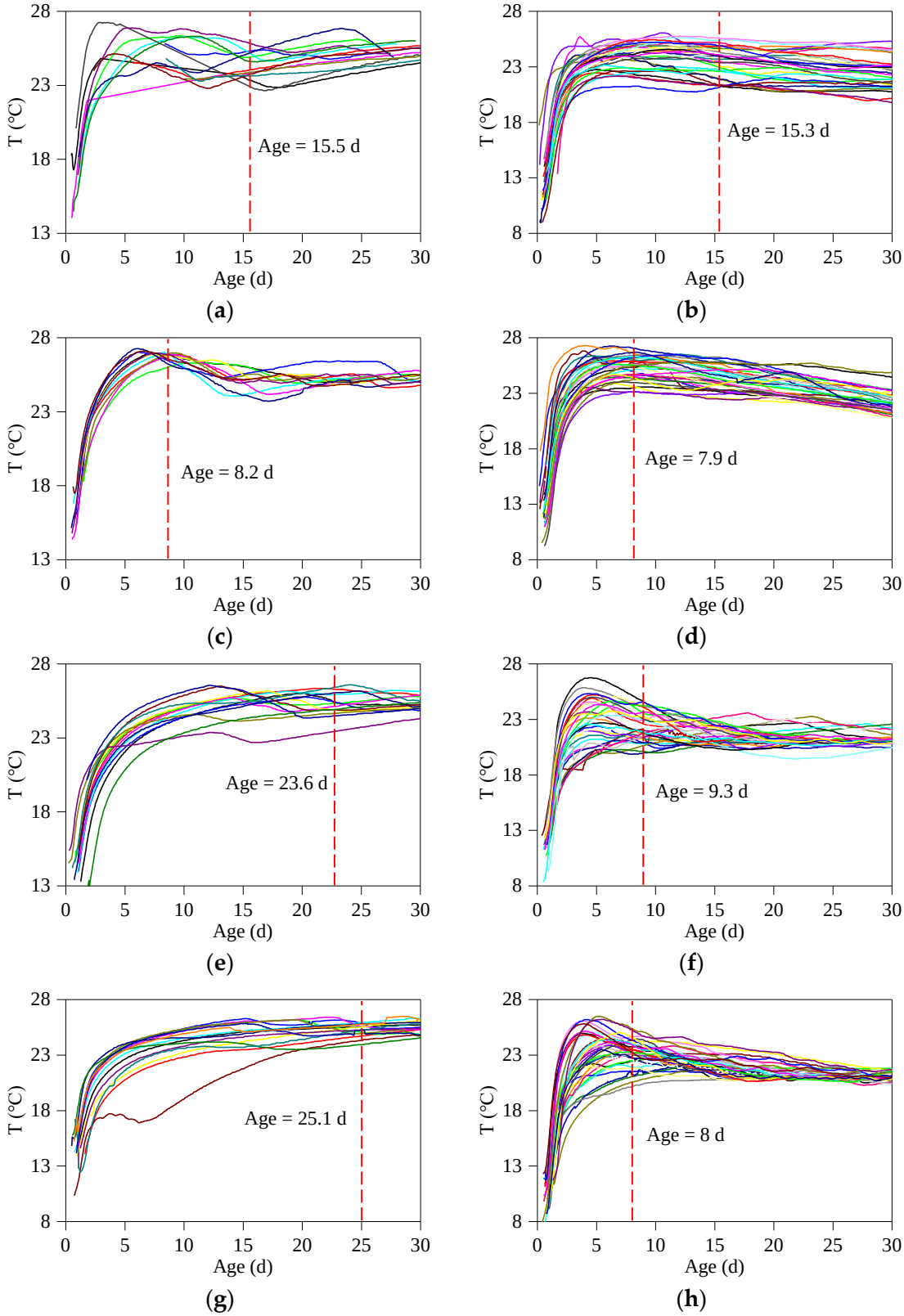

Figure 11. The temperature change curves of WDD concrete blocks: (**a**) July 2017; (**b**) July 2019; (**c**) August 2017; (**d**) August 2019; (**e**) November 2017; (**f**) November 2019; (**g**) December 2017; (**h**) December 2019. *Note: the ages in Figure 11 are the average age at which the concrete blocks reached the maximum temperature.*

Table 6. Statistics of the highest temperature of concrete blocks of the WDD dam.

Time	The Highest Temperature			
	Age (d)	Max. (°C)	Min. (°C)	Average (°C)
July and August 2017	15.5 (8.2)	27.3	25.7	26.55
July and August 2019	15.3 (7.9)	27.3	21.3	24.84
November and December 2017	23.6 (25.1)	26.6	25	26.09
November and December 2019	9.3 (8.0)	26.76	20.24	23.36

Note: The ages in brackets indicate the ages at which the highest temperature was reached in August and December.

4.3. Effect of the CTF on the Concrete Compressive Strength

A comparison of the compressive strength at the age of 28d between the four-grade concrete, three-grade concrete and the core samples from the WDD dam is shown in Figure 12. The results showed the following:

(1) the compressive strengths of 0X, 1X and 60X concrete specimens were 24.9 MPa, 26.9 MPa and 31.3 MPa, respectively. The CTF content was proportional to the compressive strength of concrete specimens, mainly because the CTF promotes the cement hydration reaction, resulting in adequate cement hydration, so the concrete strength increases accordingly. When the CTF content was 1X and 60X, the concrete strength was increased by 2 MPa and 6.4 MPa, respectively, compared with the specimens without CTF. The percentage increases were 8.0% and 25.7%;

(2) the variation range of the compressive strength of four-grade concrete specimens with the CTF content (maximum variation 25.7%) was greater than that of the three-grade concrete specimens (maximum variation 3.6%). However, the compressive strength of both grade concrete specimens increased with the CTF contents;

(3) the compressive strength of the four-grade concrete specimens without CTF was consistent with the experimental results of the dam concrete core samples, with the maximum relative error of only 2.8%. The results indicate that the CTF in the WDD dam would have little effect on the concrete strength, which is close to the condition without CTF.

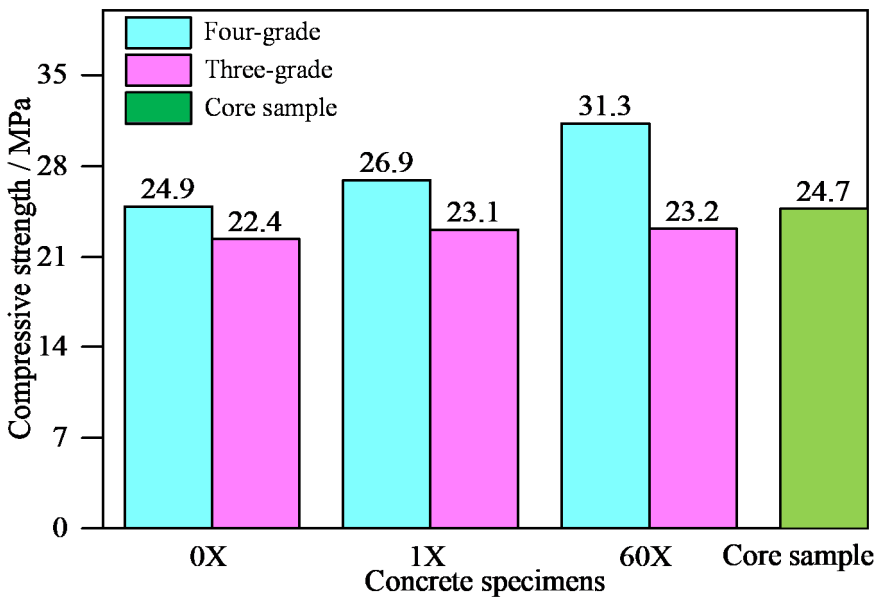

Figure 12. Comparison of compressive strength between four-grade concrete, three-grade concrete and core samples from the WDD dam.

5. Conclusions

In this study, the effects of CTF on low-heat cement hydration, concrete temperature and strength were investigated. The following conclusions can be drawn based on the studies performed.

(1) The CTF has the same chemical composition as the limestone component, except for the low-crystalline graphite (less than 10%), based on observations of hand specimens, rock slice identifications and XRF analyses.
(2) The CTF can promote an increase in the first exothermic peak of cement hydration of up to 56.7% (at 60X content) but exerts a lowering effect on the second exothermic peak of cement hydration by up to −1.3% (at 60X content). The greater the CTF content, the greater the hydration heat release. A maximum heat release increase of 3.6% was observed at 72 h (at 100X content).
(3) The highest temperature of the concrete blocks containing more CTF content (2017) was generally higher than that of the concrete blocks containing less CTF content (2019) by about 1.71 °C (July and August) and 2.73 °C (November and December), which demonstrates that the CTF could promote the increased release of heat from cement hydration.
(4) The compressive strength of concrete specimens was proportional to the CTF content; the concrete strengths of 1X and 60X CTF content were 8% and 25.7% higher, respectively, than that of 0X. In addition, the results suggest that the CTF in the WDD dam would have little effect on the concrete strength, which is close to the condition without CTF.
(5) Considering the influence of the CTF on cement hydration heat and concrete compressive strength, it is suggested that the CTF content of concrete should be controlled within 1X in practical engineering.

Author Contributions: Conceptualization, H.P. and P.L.; methodology, H.P. and P.L.; validation, P.L., Y.X., J.H. and Z.Y.; investigation, J.H. and Z.Y.; data curation, J.H. and Z.Y.; writing—original draft preparation, H.P.; writing—review and editing, P.L. and Y.X.; supervision, P.L.; project administration, P.L., J.H. and Z.Y.; funding acquisition, P.L. All authors have read and agreed to the published version of the manuscript.

Funding: This research was funded by the National Natural Science Foundation of China (Grant No: 51979146).

Institutional Review Board Statement: Not applicable.

Informed Consent Statement: Not applicable.

Data Availability Statement: All data generated or appearing in this study are available upon request from the corresponding author.

Acknowledgments: This research work was supported by the China Three Gorges Corporation Research Program (WDD/0490, WDD/0578) and Three Gorges Geotechnical Consultants CO., Ltd. Research Program (HT-2019-WW-028). The authors wish to express their gratitude for the financial support that has made this study possible.

Conflicts of Interest: The authors declare no conflict of interest.

References

1. Lin, P.; Liu, H.; Li, Q.; Hu, H. Effects of Outlets on Cracking Risk and Integral Stability of Super-High Arch Dams. *Sci. World J.* **2014**, *2014*, 312827. [CrossRef] [PubMed]
2. Lin, P.; Zhou, W.; Liu, H. Experimental Study on Cracking, Reinforcement, and Overall Stability of the Xiaowan Super-High Arch Dam. *Rock Mech. Rock Eng.* **2015**, *48*, 819–841. [CrossRef]
3. Duffaut, P. The traps behind the failure of Malpasset arch dam, France, in 1959. *J. Rock Mech. Geotech. Eng.* **2013**, *5*, 335–341. [CrossRef]
4. Lin, P.; Ma, T.; Liang, Z.; Tang, C.A.; Wang, R. Failure and overall stability analysis on high arch dam based on DFPA code. *Eng. Fail Anal.* **2014**, *45*, 164–184. [CrossRef]

5. Adams, M.P.; Ideker, J.H. Influence of aggregate type on conversion and strength in calcium aluminate cement concrete. *Cement Concrete Res.* **2017**, *100*, 284–296. [CrossRef]
6. Vishalakshi, K.P.; Revathi, V.; Sivamurthy Reddy, S. Effect of type of coarse aggregate on the strength properties and fracture energy of normal and high strength concrete. *Eng. Fract. Mech.* **2018**, *194*, 52–60. [CrossRef]
7. Gautam, B.P.; Panesar, D.K.; Sheikh, S.A.; Vecchio, F.J. Effect of coarse aggregate grading on the ASR expansion and damage of concrete. *Cement Concrete Res.* **2017**, *95*, 75–83. [CrossRef]
8. Elices, M.; Rocco, C.G. Effect of aggregate size on the fracture and mechanical properties of a simple concrete. *Eng. Fract. Mech.* **2008**, *75*, 3839–3851. [CrossRef]
9. Rocco, C.G.; Elices, M. Effect of aggregate shape on the mechanical properties of a simple concrete. *Eng. Fract. Mech.* **2009**, *76*, 286–298. [CrossRef]
10. Zhou, C.; Shu, X.; Huang, B. Predicting concrete coefficient of thermal expansion with an improved micromechanical model. *Constr. Build. Mater.* **2014**, *68*, 10–16. [CrossRef]
11. Piotrowska, E.; Forquin, P.; Malecot, Y. Experimental study of static and dynamic behavior of concrete under high confinement: Effect of coarse aggregate strength. *Mech. Mater.* **2016**, *92*, 164–174. [CrossRef]
12. Castro, N.; Wigum, B.J. Assessment of the potential alkali-reactivity of aggregates for concrete by image analysis petrography. *Cement Concrete Res.* **2012**, *42*, 1635–1644. [CrossRef]
13. Sanchez, L.F.M.; Fournier, B.; Jolin, M.; Mitchell, D.; Bastien, J. Overall assessment of Alkali-Aggregate Reaction (AAR) in concretes presenting different strengths and incorporating a wide range of reactive aggregate types and natures. *Cement Concrete Res.* **2017**, *93*, 17–31. [CrossRef]
14. Rößler, C.; Möser, B.; Giebson, C.; Ludwig, H.M. Application of Electron Backscatter Diffraction to evaluate the ASR risk of concrete aggregates. *Cement Concrete Res.* **2017**, *95*, 47–55. [CrossRef]
15. Iskhakov, T.; Timothy, J.J.; Meschke, G. Expansion and deterioration of concrete due to ASR: Micromechanical modeling and analysis. *Cement Concrete Res.* **2019**, *115*, 507–518. [CrossRef]
16. Ye, G.; Liu, X.; De Schutter, G.; Poppe, A.M.; Taerwe, L. Influence of limestone powder used as filler in SCC on hydration and microstructure of cement pastes. *Cem. Concr. Compos.* **2007**, *29*, 94–102. [CrossRef]
17. Lothenbach, B.; Le Saout, G.; Gallucci, E.; Scrivener, K. Influence of limestone on the hydration of Portland cements. *Cement Concrete Res.* **2008**, *38*, 848–860. [CrossRef]
18. Fediuk, R.; Timokhin, R.; Mochalov, A.; Otsokov, K.; Lashina, I. Performance Properties of High-Density Impermeable Cementitious Paste. *J. Mater. Civil. Eng.* **2019**, *31*, 4019013. [CrossRef]
19. Zhang, D.; Cai, X.; Hu, L. Effect of Curing Temperature on Hydration of Calcium Aluminate Cement-Calcium Sulfate-Limestone System. *J. Mater. Civil. Eng.* **2018**, *30*, 6018011. [CrossRef]
20. Thongsanitgarn, P.; Wongkeo, W.; Chaipanich, A.; Poon, C.S. Heat of hydration of Portland high-calcium fly ash cement incorporating limestone powder: Effect of limestone particle size. *Constr. Build. Mater.* **2014**, *66*, 410–417. [CrossRef]
21. Vance, K.; Aguayo, M.; Oey, T.; Sant, G.; Neithalath, N. Hydration and strength development in ternary portland cement blends containing limestone and fly ash or metakaolin. *Cem. Concr. Compos.* **2013**, *39*, 93–103. [CrossRef]
22. Angulski Da Luz, C.; Hooton, R.D. Influence of Supersulfated Cement Composition on Hydration Process. *J. Mater. Civil Eng.* **2019**, *31*, 04019090. [CrossRef]
23. Wang, S.; Chen, C.; Lu, L.; Cheng, X. Effects of slag and limestone powder on the hydration and hardening process of alite-barium calcium sulphoaluminate cement. *Constr. Build. Mater.* **2012**, *35*, 227–231. [CrossRef]
24. Wu, Q.; Wang, S.; Yang, T.; Zhu, H.; Li, S. Effect of High-Magnesium Nickel Slag on Hydration Characteristics of Portland Cement. *J. Mater. Civil Eng.* **2019**, *31*, 04019051. [CrossRef]
25. Tang, J.; Deng, M.; Wang, A.; Xie, L. Influence of the Cement Fineness on Strengths of Cement Pastes Containing High Phosphorus Slag. *J. Mater. Civil Eng.* **2015**, *27*, 04015047. [CrossRef]
26. Klemczak, B.; Batog, M. Heat of hydration of low-clinker cements. *J. Therm. Anal. Calorim.* **2016**, *123*, 1351–1360. [CrossRef]
27. Kumar, M.; Singh, S.K.; Singh, N.P. Heat evolution during the hydration of Portland cement in the presence of fly ash, calcium hydroxide and super plasticizer. *Thermochim. Acta* **2012**, *548*, 27–32. [CrossRef]
28. Singh, N.B.; Kalra, M.; Kumar, M.; Rai, S. Hydration of ternary cementitious system: Portland cement, fly ash and silica fume. *J. Therm. Anal. Calorim.* **2015**, *119*, 381–389. [CrossRef]
29. Sakai, E.; Miyahara, S.; Ohsawa, S.; Lee, S.; Daimon, M. Hydration of fly ash cement. *Cement Concrete Res.* **2005**, *35*, 1135–1140. [CrossRef]
30. Thongsanitgarn, P.; Wongkeo, W.; Chaipanich, A. Hydration and Compressive Strength of Blended Cement Containing Fly Ash and Limestone as Cement Replacement. *J. Mater. Civil. Eng.* **2014**, *26*, 04014088. [CrossRef]
31. Bentz, D.P.; Ferraris, C.F.; Jones, S.Z.; Lootens, D.; Zunino, F. Limestone and silica powder replacements for cement: Early-age performance. *Cem. Concr. Compos.* **2017**, *78*, 43–56. [CrossRef] [PubMed]
32. Siler, P.; Kratky, J.; De Belie, N. Isothermal and solution calorimetry to assess the effect of superplasticizers and mineral admixtures on cement hydration. *J. Therm. Anal. Calorim.* **2012**, *107*, 313–320. [CrossRef]
33. Li, W.; Li, X.; Chen, S.J.; Liu, Y.M.; Duan, W.H.; Shah, S.P. Effects of graphene oxide on early-age hydration and electrical resistivity of Portland cement paste. *Constr. Build. Mater.* **2017**, *136*, 506–514. [CrossRef]

34. Lu, Z.; Li, X.; Hanif, A.; Chen, B.; Parthasarathy, P.; Yu, J.; Li, Z. Early-age interaction mechanism between the graphene oxide and cement hydrates. *Constr. Build. Mater.* **2017**, *152*, 232–239. [CrossRef]
35. Hu, J.; Wu, Y.; Li, G.; Liu, S.; Peng, H.; Wan, L.; Lu, Y.; Wang, C. Influence of carbonaceous thin film in limestone aggregate on concrete performance. *Yangtze River* **2021**, *52*, 214–219. [CrossRef]
36. Peng, S.; Yang, X.; Niu, Y.; Yang, B.; Li, J. Influence of Artificial Aggregate on Concrete Gas Content in Shuibuya Hydropower Station. *Yangtze River* **2007**, *38*, 99–100. [CrossRef]
37. Xiang, J.S. Review on Difficulties in Construction and Operation of Sand and Stone Processing System in Liyang Pumped Storage Power Station. *Hunan Hydro Power* **2018**, *1*, 68–70.
38. Wang, F.; Gong, A.; Peng, Y.; Zhao, D. Application Study on Durability of Silica Fume Concrete in Fengweihe Hydropower Station. *J. Yunnan Agric. Univ.* **2011**, *26*, 105–109. [CrossRef]
39. Han, F.; Liu, R.; Wang, D.; Yan, P. Characteristics of the hydration heat evolution of composite binder at different hydrating temperature. *Thermochim Acta.* **2014**, *586*, 52–57. [CrossRef]
40. Taylor, H.F.W. *Cement Chemistry*; Academic Press: Cambridge, MA, USA, 1997.
41. Hou, D.; Lu, Z.; Li, X.; Ma, H.; Li, Z. Reactive molecular dynamics and experimental study of graphene-cement composites: Structure, dynamics and reinforcement mechanisms. *Carbon* **2017**, *115*, 188–208. [CrossRef]
42. Oey, T.; Kumar, A.; Bullard, J.W.; Neithalath, N.; Sant, G. The Filler Effect: The Influence of Filler Content and Surface Area on Cementitious Reaction Rates. *J. Am. Ceram. Soc.* **2013**, *96*, 1978–1990. [CrossRef]
43. Tikkanen, J.; Cwirzen, A.; Penttala, V. Effects of mineral powders on hydration process and hydration products in normal strength concrete. *Constr. Build. Mater.* **2014**, *72*, 7–14. [CrossRef]
44. Kakali, G.; Tsivilis, S.; Aggeli, E.; Bati, M. Hydration products of C_3A, C_3S and Portland cement in the presence of $CaCO_3$. *Cement Concrete Res.* **2000**, *30*, 1073–1077. [CrossRef]